AIAA SciTech Forum
6-10 January 2020, Orlando, FL
AIAA Scitech 2020 Forum

10.2514/6.2020-0517

Ultrafast Laser-Absorption Spectroscopy in the Mid-Infrared for Measuring Temperature and Species in Combustion Gases

Ryan J. Tancin *, Vishnu Radhakrishna †, Ziqiao Chang†, Mingming Gu†, Robert P. Lucht ‡ and Christopher S. Goldenstein §
Purdue University, West Lafayette, IN, 47907, United States

This manuscript presents the development and application of an ultrafast (femtosecond) laser-absorption-spectroscopy (ULAS) diagnostic for measuring temperature, CO and CO_2 in combustion gases. An 80 MHz Ti:Sapphire oscillator was used to generate ultrafast (55 fs) pulses of light centered at a wavelength of 800 nm. An ultrafast amplifier was used to increase the pulse energy to 2 mJ which reduced the repetition rate to 5 kHz. The pulses were then converted to the mid-infrared using optical-parametric amplification (OPA) and non-collinear difference-frequency generation (NDFG). The broadband, mid-IR pulses of light were then passed through an absorbing gas and focused into a high-speed mid-infrared spectrograph to provide spectrally and spatially (in 1D) resolved, single-shot images of the transmitted light intensity at 5 kHz. Wavelengths near 4975 nm and 4186 nm were used to measure spectra of CO and CO_2, respectively, with a spectral bandwidth and resolution near 30 and 0.3 nm, respectively. This diagnostic was demonstrated with single-shot, single-spectrum (i.e., no-spatial averaging) measurements of temperature, CO, and CO_2 column density at a repetition rate of 5 kHz in laser-ignited HMX flames. Measurements for each species were acquired at the same location in the flame, under identical conditions. The results demonstrate that this diagnostic can provide single-shot temperature measurements via CO or CO_2 with a time resolution less than 1 picosecond and a 1-σ precision of ≈1-2%. Species-specific differences in the measured path-integrated temperature were used to provide additional insight into the structure of HMX flames burning in air.

I. Nomenclature

c	=	speed of light in a vacuum (cm s^{-1})
E''	=	lower-state energy (cm^{-1})
FWHM	=	Full Width at Half Maximum
h	=	Planck's constant (Js)
I_o	=	incident (i.e., baseline) laser intensity at camera-spectrograph resolution (a.u.)
$I_{o,HR}$	=	baseline laser intensity at high resolution (a.u.)
$I_{o,HR,conv}$	=	baseline laser intensity post convolution with the IRF at high resolution (a.u.)
I_t	=	transmitted laser intensity at camera-spectrograph resolution (a.u.)
$I_{t,HR,conv}$	=	transmitted laser intensity post convolution with the IRF at high resolution (a.u.)
IRF	=	Instrument Response Function
k_B	=	Boltzmann constant (J/molecule-K)
L	=	optical path length through absorbing gas (cm)
NDFG	=	Non-collinear Difference-Frequency Generation
OPA	=	Optical-Parametric Amplification
P	=	pressure (atm)
Q	=	partition function sum (pure)
S	=	transition linestrength (cm^{-2}/atm)
T	=	temperature (K)

*Graduate Student, School of Aeronautics and Astronautics
†Graduate Student, School of Mechanical Engineering
‡Ralph and Bettye Bailey Distinguished Professor of Mechanical Engineering, School of Mechanical Engineering and AIAA Fellow
§Assistant Professor, School of Mechanical Engineering

T_0	=	reference temperature (296 K)
T_{CO}	=	temperature measured from path-integrated absorbance spectra of CO (K)
T_{CO_2}	=	temperature measured from path-integrated absorbance spectra of CO_2 (K)
$\alpha(\nu)$	=	spectral absorbance
$\alpha_{HR}(\nu)$	=	simulated absorbance at high resolution prior to convolution with the IRF (pure)
$\alpha_{HR,conv}(\nu)$	=	simulated absorbance at high resolution after convolution with the IRF (pure)
$\alpha_{conv}(\nu)$	=	simulated absorbance at camera-spectrograph resolution after convolution with the IRF (pure)
λ	=	optical wavelength (nm)
ν	=	optical frequency (cm^{-1})
ν_o	=	linecenter frequency (cm^{-1})
$\phi(\nu)$	=	transition lineshape (cm)
χ	=	species mole fraction
$\chi_{abs}L$	=	absorbing-species column density (cm)

II. Introduction

LASER-absorption spectroscopy (LAS) is widely used to provide quantitative, non-intrusive temperature and species measurements in combustion environments [1]. Many LAS techniques such as scanned-wavelength direct-absorption spectroscopy (scanned-DA) and wavelength-modulation spectroscopy (WMS) employ narrowband, wavelength-tunable lasers such as tunable diode lasers (TDLs), quantum-cascade lasers (QCLs), and interband cascade lasers (ICLs). The wavelength of these lasers can be scanned via injection-current tuning across a relatively narrow frequency range (typically < 3 cm^{-1} at kHz rates), thereby limiting them to measuring only a few absorption transitions at high rates [1]. Further, the time resolution of such techniques is limited by the speed at which the laser can be tuned across the absorption features of interest (typically on the order of 1 ms to 1 μs) [2, 3].

In contrast, diagnostics utilizing broadband light sources or with high wavelength tunability can achieve a spectral bandwidth of 10s to 1000s cm^{-1} [4–11]. This enables 10s to 10000s of discrete absorption features to be measured simultaneously. As a result, such diagnostics offer several advantages. For example, broadband diagnostics can provide an increased operating range since numerous transitions with different lower-state energies (and therefore temperature sensitivity) can be measured simultaneously [12]. Their larger spectral bandwidth also facilitates simultaneous measurements of multiple species. Further, increased spectral bandwidth may facilitate measurements of species with broad or blended spectra, such as the spectra of gases at high pressure or that of large (>4 atoms) molecular gases. For these reasons, numerous researchers have developed a variety of broadband LAS diagnostics.

Lasers with broad wavelength-tuning capabilities such as vertical-cavity surface-emitting lasers (VCSELs) and external-cavity quantum-cascade lasers have been used for broadband LAS measurements in a variety of applications. For example, VCSELs were used by Sanders et al. [4] to measure temperature and O_2 near 760 nm with >30 cm^{-1} of bandwidth, and Rein et al. [5] used a MEMS VCSEL emitting near 1.4 μm with ≈170 cm^{-1} of bandwidth to obtain measurements of H_2O and temperature at 100 kHz. In addition, an external-cavity quantum-cascade laser was recently used to acquire measurements of C_2H_4 with 100 cm^{-1} of bandwidth near 8.5 μm and 11.7 μm [6].

Ultrafast lasers have also been utilized for broadband absorption measurements. For example, a supercontinuum light-source driven by an ultrafast laser was used by Sanders [7] to measure temperature and multiple species using 1000 cm^{-1} of bandwidth near 1450 nm. Similarly, Blume and Wagner [8] used a commercial supercontinuum source with 110 cm^{-1} of bandwidth near 1655 nm to measure temperature and CH_4 in a burner flame. In addition, a dual-frequency-comb spectrometer with 160 cm^{-1} of bandwidth near 1655 nm has been used to measure temperature and CH_4 in a rapid-compression machine [10]. Recently, a background-free absorption-spectroscopy technique called time-resolved, optically gated absorption (TOGA) spectroscopy was developed and used to measure OH spectra near 310 nm with 300 cm^{-1} of bandwidth [11]. This diagnostic provided single-shot measurements of ultraviolet spectra with a time resolution less than 10 ps.

Most recently, we demonstrated the first (to our knowledge) mid-infrared, single-shot, ultrafast (femtosecond) laser-absorption measurements of temperature and species in combustion gases. Specifically, measurements of temperature, CO, and CH_4 were acquired in flames with a repetition rate of 5 kHz and time resolution estimated to be less than 1 picosecond (after accounting for dispersion) [13]. This diagnostic offers several advantages compared to alternative broadband LAS diagnostics. Perhaps most significantly, the time resolution of the diagnostic is at least 6 orders of magnitude faster than previously reported infrared LAS diagnostics applied to combustion gases, albeit with a lower measurement repetition rate compared to some TDL-, QCL-, and VCSEL-based diagnostics [1]. In addition, by utilizing

a high-density, 2D focal plane array as the detector, this diagnostic offers the potential to provide high-resolution 1D measurements of absorbance spectra and, therefore, thermochemical flame structure similar to recently developed scanned-wavelength laser-absorption-imaging diagnostics [14, 15].

The work presented here builds on our recently developed mid-infrared ultrafast-laser-absorption diagnostics [13] by: 1) extending the diagnostic to single-shot measurements of temperature and CO_2 and 2) refining the optical setup to enable the first mid-infrared, single-shot, *single-spectrum* (i.e., no spatial averaging of spectra) measurements of temperature and species with ultrafast time resolution. This diagnostic was applied to acquire measurements of temperature, CO and CO_2 at 5 kHz in laser-ignited HMX (i.e., 1,3,5,7-tetranitro-1,3,5,7-tetrazoctane) flames. The results demonstrate that species-specific differences in the temperature inferred from the path-integrated absorbance spectra of CO and CO_2 can be utilized to gain additional insight into the structure of HMX flames burning in air.

III. Wavelength and Species Selection

CO and CO_2 were chosen for the application of this diagnostic because they are key combustion products of many propellants and hydrocarbon fuels. Further, they are both often present in concentrations that are sufficient for high-fidelity measurements of temperature in many flames and combustion gases of practical importance. Last, comparing temperature measurements acquired via an intermediate species (e.g., CO) and a complete combustion product (e.g., CO_2) can provide improved insight into the homogeneity of the combustion gas.

For measurements of CO_2 spectra, care was taken to choose a spectral window which has high temperature sensitivity and weak absorbance at ambient temperature, the latter is necessary to avoid strong absorbance from ambient CO_2 since the optical path length through the air was nearly 4 m. As a result, a spectral window centered at 4186 nm (2389 cm^{-1}) was used to measure high lower-state-energy transitions near the bandhead of CO_2's fundamental asymmetric-stretch vibration band. Recent work has shown that this region of CO_2's absorbance spectrum provides high-temperature sensitivity at flame conditions and provides access to well-isolated absorption transitions [16].

For measurements of CO spectra, wavelengths near 4975 nm (2010 cm^{-1}) were used to access strong, well isolated, high lower-state-energy transitions in CO's P-branch which exhibit minimal interference with H_2O and CO_2 transitions [17]. Compared to our prior work [13, 14], longer wavelengths were used to access P-branch transitions with even larger lower-state energy. This was done to further desensitize the absorption measurements to boundary layers.

IV. Experimental Details

Fig. 1 shows a schematic summarizing the experimental setup and data-processing procedure. Ultrafast pulses of light were generated using a mode-locked, Coherent Mantis Ti:Sapphire laser at a rate of 80 MHz and a center wavelength of 800 nm. The pulses were then tailored for amplification by a FemtoJock pulse-shaper, before being directed to a Coherent Legend Elite Duo amplifier (regenerative, multi-stage). The amplifier outputs 55 fs duration pulses with a pulse energy of 2 mJ at a rate of 5 kHz. Next, pulses were passed into an OPA module (Coherent OPerA Solo) which used NDFG crystals to convert the amplified pulses into the mid-IR. Output wavelengths centered from 2.5 to 4.9 μm or 4 to 16 μm can be achieved using one of two DFG crystals. Each pulse contained $\approx$600 cm^{-1} of spectral bandwidth that is usable for laser-absorption measurements. The center wavelength of the OPA output was selected through the OPerA Solo software which controls the manipulation of the NDFG crystals through servos to output the desired wavelength. In this work, pulses were centered at 4.2 μm and 4.9 μm and had corresponding pulse energies of 14 μJ and 4 μJ, respectively.

Downstream of the OPA, the mid-IR beam was directed through a Rochon prism polarizer to achieve the desired pulse energy (adjusted by rotating the polarizer) and prevent the IR camera from saturating. The ordinary ray was used for absorption measurements and the extraordinary ray was directed to a beam dump. Prior to being passed through the test gas, the $1/e^2$ beam diameter was reduced from $\approx$7 mm to $\approx$800 μm using a lens telescope consisting of a CaF_2 plano-convex lens (f = 200 mm) to focus the beam and a Si plano-convex lens (f = 25.4 mm, 2-5 μm AR coating) to collimate the output beam. Since the output beam from the OPA has a relatively low quality factor (beam was noticeably elliptical), a 200 μm pinhole was placed at the focal point of the f = 200 mm lens. This improved the beam quality by acting as a spatial filter (i.e., rejecting the non-gaussian components of the laser beam). In turn, this enabled tighter collimation of the beam and tighter focusing of the beam onto the slit of the spectrograph. This ultimately improved the spatial and spectral resolution of the diagnostic. After passing through the absorbing gas, the beam was expanded using a second lens telescope. The purpose of this telescope was to increase the laser beam diameter such that the beam could be focused to a smaller waist on the spectrograph slit, ultimately providing improved spectral resolution. This

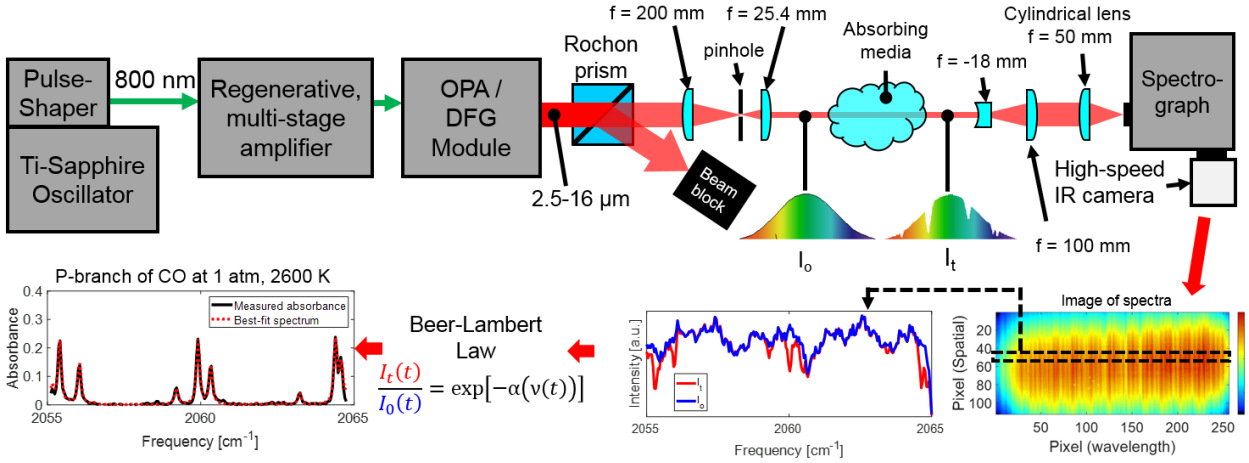

Fig. 1 Schematic illustrating the ultrafast laser system, optical setup and general data-processing procedures.

telescope consisted of a CaF_2, plano-concave lens (f = -18 mm, 2-5 μm AR coating) to expand the laser beam and a CaF_2, plano-convex lens (f = 100 mm, 2-5 μm AR coating) to collimate the beam. The input beam to this telescope had a $1/e^2$ diameter of ≈2 mm and an output $1/e^2$ beam diameter of ≈11 mm. A final ZnSe plano-convex cylindrical lens (f = 50 mm) focused the beam in one dimension onto the slit of the spectrograph.

An Andor Shamrock 500i imaging spectrometer with a 300 line/mm diffraction grating was used to spectrally disperse the ultrafast pulses onto the focal plane array of a high-speed mid-IR camera (Telops Fast-IR 2k). In this work, images were acquired using a 44 x 320 pixel window and an integration time of 5 μs. The x-dimension (320 pixels) of the camera images corresponds to wavelength and the y-dimension (44 pixels) corresponds to vertical position within the beam of ultrafast pulses. The camera timing was synchronized with the ultrafast laser and images were acquired at 10 kHz (twice the repetition rate of the laser) such that background signal (e.g., from camera dark current, ambient emission and flame emission) could be recorded in between pulses. In post processing, the most recent background image was subtracted off of each image of an ultrafast pulse.

All measurements presented in this work were acquired in HMX flames burning in air at atmospheric pressure. Example images (taken with a Nikon D3200 DSLR) of an HMX flame at various times after ignition are shown in Fig. 2. In all tests, pellets of pressed HMX (6 mm diameter, 3.6 mm ± 0.1 mm tall) were used. The HMX was ignited using a CO_2 laser emitting an intensity of 78 W/cm^2 at 10.6 μm, and the pellets were laser-heated throughout the duration of the test. Measurements of temperature, CO, and CO_2 were acquired 6 mm above the initial surface location of the HMX pellet. Data acquisition began 100 ms before the CO_2 laser was turned on to allow for the baseline laser intensity to be recorded.

V. Data Processing Procedure

The data-processing procedure and spectral-fitting routine employed in this work are thoroughly described in our recent manuscript [13]. The most pertinent details are repeated here for clarity and several minor changes are discussed. Beer's law (Eq. 1) was used to calculate the measured spectral absorbance (α) which is influenced by instrument broadening (later accounted for in the spectral-fitting routine).

$$\alpha(\nu) = -ln(I_t(\nu)/I_o(\nu)) \tag{1}$$

The baseline laser intensity (I_o) was constructed by averaging together 250 images of laser pulses (to mitigate pixel noise) which were recorded in the absence of the test gas. Although the camera records 44 spectra (I_o or I_t) for each laser pulse, only one spectrum of I_t was utilized to demonstrate the single-shot, single-spectrum SNR of the diagnostic and, therefore, demonstrate this diagnostic's potential to provide 1D-resolved measurements of absorbance spectra.

Gas properties were extracted from the data by least-squares fitting a simulated absorbance spectrum to the measured absorbance spectrum using a nonlinear spectral-fitting routine employing the Levenberg–Marquardt algorithm. In order to properly account for instrument broadening induced by the spectrograph, the spectral absorbance was modeled according to the following procedure. First, the absorbance spectrum was simulated at high resolution (0.0005 cm^{-1}

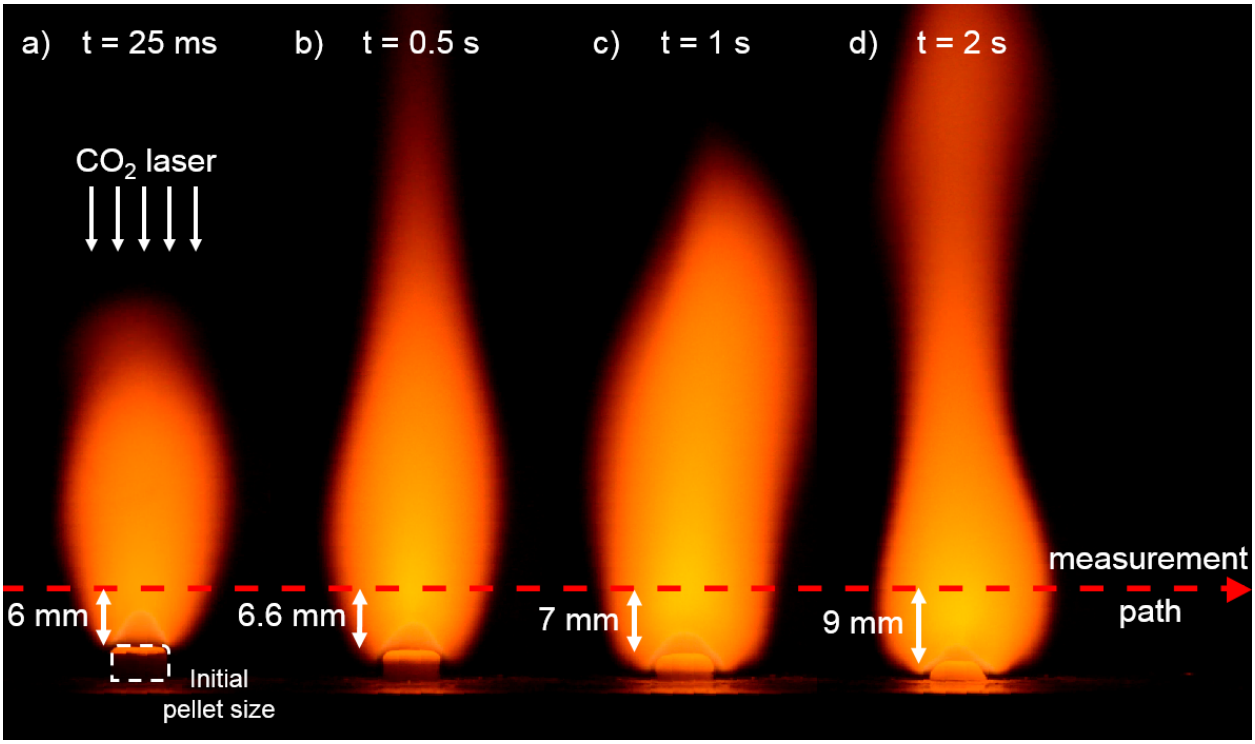

Fig. 2 Images of CO_2-laser-ignited HMX flames taken with a Nikon D3200 at 60 FPS. The images shown correspond to the results presented in Figure 3. Select frames are shown corresponding to a) 25 ms, b) 0.5 s, c) 1 s and d) 2 s after ignition. The images illustrate the variation in flame structure due to the low frequency (≈11 Hz) instability.

here) without instrument broadening using Eq. 2 which invokes the isolated line approximation and, thus, ignores linemixing.

$$\alpha_{HR}(\nu) = \sum_j S_j(T)\phi_j(\nu)P\chi L \tag{2}$$

The pertinent spectroscopic parameters were taken from the HITEMP2010 [18] and HITEMP2019 [19] databases for CO_2 and CO, respectively. The transition lineshapes were modeled using a Voigt profile and the transition linestrengths at a given temperature were calculated using Eq. 3.

$$S_j(T) = S_j(T_o)\frac{Q(T_o)}{Q(T)}\frac{T_o}{T}\exp\left[-\frac{hcE_j''}{k_B}\left(\frac{1}{T}-\frac{1}{T_o}\right)\right]\left[1-\exp\left(\frac{-hc\nu_o}{k_BT}\right)\right]\left[1-\exp\left(\frac{-hc\nu_o}{k_BT_o}\right)\right]^{-1} \tag{3}$$

Next, the measured baseline (I_o) was linearly interpolated to match the frequency axis of the high-resolution simulation of α_{HR}, thereby yielding $I_{o,HR}$. Subsequently, α_{HR} and $I_{o,HR}$ were used to create a "semi-empirical" transmission spectrum using Beer's law which was then convolved with the IRF of the spectrograph-camera system using Eq. 4 to produce $I_{t,HR,conv}$.

$$I_{t,HR,conv}(\lambda) = \int_{-\infty}^{\infty} IRF(\lambda-\tau)I_{o,HR}(\tau)e^{-\alpha_{HR}(T,P,\chi,L)}d\tau \tag{4}$$

$I_{o,HR}$ was then convolved with the IRF to yield $I_{o,HR,conv}$. Next, Beer's law was used with $I_{o,HR,conv}$ and $I_{t,HR,conv}$ as inputs to calculate the simulated absorbance spectrum with instrument broadening accounted for ($\alpha_{HR,conv}$). Finally, $\alpha_{HR,conv}$ was downsampled to the same frequency axis as I_o to produce α_{conv} which was then directly compared to the measured absorbance spectrum to evaluate the sum-of-squared error and guide the next iteration of the spectral-fitting routine. It is important to note that the IRF is not directly convolved with $\alpha_{HR}(\nu)$ because the spectrograph-camera system "sees" transmitted intensity, not absorbance.

The IRF used in this work was modeled as the weighted sum of a Gaussian and Lorentzian distribution. The convolution in Eq. 4 was executed in wavelength space since the FWHM of the IRF is constant in wavelength space and not frequency space.

The following parameters were floated in the spectral-fitting routine: 1) gas temperature, 2) absorbing-species column density ($\chi_{abs}L$), 3) a linear (i.e., 2 parameter) baseline intensity correction (to account for beam steering and shot-to-shot fluctuations in the pulse energy), 4) the linecenter frequencies for several prominent spectral lines, 5) the FWHM of the empirical IRF, and 6) the relative weight between the Gaussian and Lorentzian components of the the IRF. The frequency axis was first estimated by matching the location of 3 prominent absorption peaks to their respective frequencies as determined by referencing simulations performed using the HITEMP2010 and HITEMP2019 databases. The fitting routine was then allowed to adjust the frequencies of the approximate chosen locations to precisely align the measured data with its frequency axis. The remainder of the frequency axis was filled in using cubic spline interpolation. The frequency axis was a nearly linear function of pixel number (≈0.1 nm/pixel). The linecenter frequencies and parameters governing the shape of the IRF were constant throughout the duration of the test. Once their values were determined by the spectral fitting routine using a reference spectrum, they were held constant throughout the remainder of the data processing.

VI. Results

This section presents ULAS measurements of temperature (from CO and CO_2) and the column density of CO and CO_2 acquired in laser-ignited HMX flames burning in air at 1 atm. Since HMX is fuel rich, HMX flames burning in air exhibit a partially premixed flame structure with a fuel-rich core surrounded by a shroud of combustion products with greater CO_2 concentration due to diffusion of atmospheric oxygen into the flame. Measurements of temperature acquired from path-integrated absorbance spectra of CO and CO_2 are both presented to highlight species-specific differences in the measured temperature which, in the limit of linearly-temperature-dependent linestrengths, is given by an absorbing-species-weighted (partial pressure or number density weighting) path-averaged temperature [20]. As a result, CO-based temperature measurements are expected to be more representative of the flame core (consisting of HMX combustion products), while CO_2-based temperature measurements will be biased more towards the surrounding shroud of HMX-air combustion products. The results presented next support these arguments.

Fig. 3(a) shows a representative single-shot measurement of CO's absorbance spectrum near 2010 cm^{-1} and its corresponding best-fit spectrum acquired 1.5 s after ignition. The measured and best-fit spectra exhibit excellent agreement with a peak-normalized residual less than 5%. The baseline 1-σ noise level in absorbance was 0.31% and the measured FWHM of the IRF for this dataset was 0.26 nm.

Fig. 3(b) shows measured time histories of CO-based temperature (T_{CO}) and $\chi_{CO}L$. Approximately 0.1 s after ignition, T_{CO} reached a maximum quasi-steady value of approximately 2800 K and as the burning surface regressed, T_{CO} decreased to 2700 K at 2 s after ignition. The 1-σ precision in temperature was 57 K (i.e., 2% of the measurement

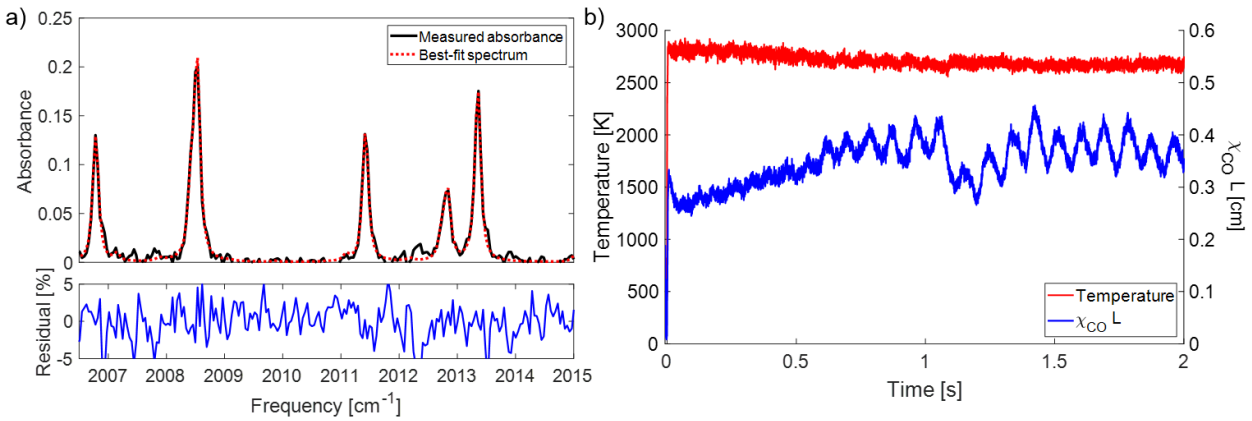

Fig. 3 (a) A representative, single-shot, single-row measurement of CO's absorbance spectrum and the best-fit spectrum acquired 1.5 s after ignition. (b) Measured time histories of T_{CO} and CO column density ($\chi_{CO}L$) acquired in a laser-ignited HMX flame.

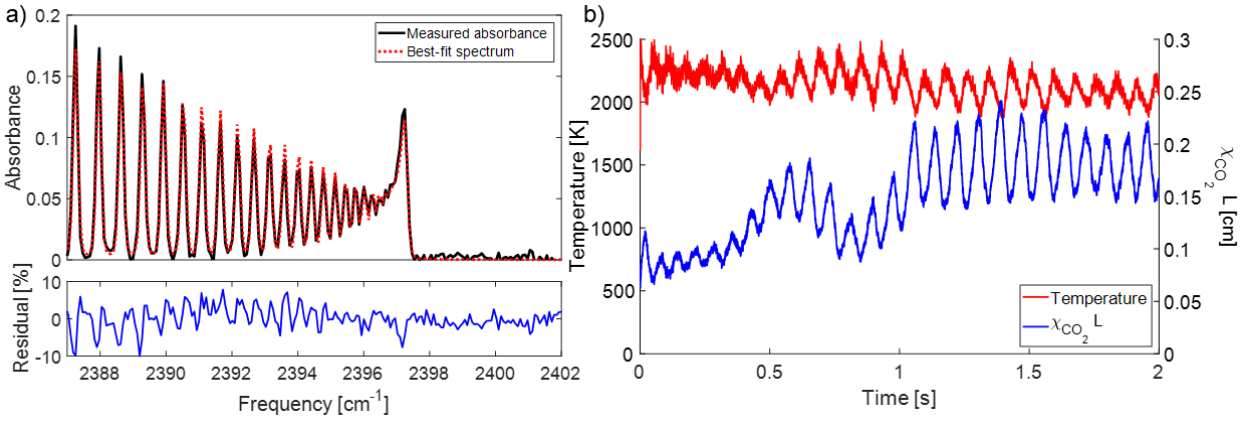

Fig. 4 (a) A representative, single-shot, single-row measurement of CO_2's absorbance spectrum and the best-fit spectrum acquired 1.5 s after ignition. (b) Measured time histories of T_{CO_2} and CO_2 column density ($\chi_{CO_2}L$ acquired in a laser-ignited HMX flame.

at 2750 K). The maximum quasi-steady value of T_{CO} is close (within 117 K) to the adiabatic flame temperature of HMX (2917 K at 1 atm) predicted by NASA CEA. While the HMX flames are not adiabatic, this suggests that the CO-based temperature measurement is not heavily influenced by line-of-sight non-uniformities and is representative of conditions in the core of the flame. It should be noted that the maximum T_{CO} is ≈130 K hotter than that previously measured in our lab at similar conditions using CO transitions near 2060 cm^{-1} [13]. This relatively minor difference is likely due to the fact that higher-energy CO transitions were measured in this work, thereby further desensitizing the measured spectra to cooler regions of flame gas that exist closer to the flame perimeter [1, 20].

The measured CO column density was ≈0.26 cm at 0.1 s after ignition and it increased steadily to a time-averaged value of 0.375 cm. The 1-σ precision in column density was 3.7% at a value of 0.375 cm. In addition, an oscillation in CO column density was observed which grew in amplitude until 1 s after ignition where the amplitude reached steady state. The measured frequency and amplitude of the oscillation were 11.1 Hz and 0.07 cm, respectively. This results from a well known and easily observed instability in flame structure [21].

Fig. 4(a) shows an example single-shot, single-row measurement of CO_2's absorbance spectrum near 2394 cm^{-1} acquired in the HMX flame 1.5 seconds after ignition. The 1-σ noise level in the measured absorbance spectrum is 0.33% and the FWHM of the IRF was 0.27 nm for the best-fit spectrum. Interestingly, the best-fit spectrum consistently under-predicts the measured absorbance for the lower-energy transitions and over-predicts the absorbance of the higher-energy transitions located closer to the bandhead, with the exception of the bandhead itself which may result from linemixing effects [22]. These differences likely result primarily from the fact that the measured CO_2 spectra are acquired over a range of temperatures (due to the path-integrated nature of LAS and the partially premixed flame structure of HMX flames in air) while the modelled spectrum is calculated at a single temperature. This suggests that line-of-sight non-uniformities in temperature significantly impact the measurements of CO_2 spectra.

Fig. 4(b) shows measured time histories of CO_2-based temperature (T_{CO_2}) and $\chi_{CO_2}L$. The mean value of T_{CO_2} is 2250 K at 0.1 s after ignition and this decreases steadily to 2050 K at 2 s after ignition. The 1-σ precision of T_{CO_2} is 27.4 K (1.2%). Unlike T_{CO}, T_{CO_2} oscillated at 12.2 Hz with an amplitude of 350 K (i.e., 16% at 2200 K). The column density of CO_2 increased from an average value of 0.8 cm shortly after ignition to 0.175 cm at approximately 1 s after ignition, after which the column density reached a plateau. The 1-σ precision of the column density measurement was 1.1% of the measured value. An oscillation in CO_2 column density was also observed at 12.2 Hz, but ≈180 degrees out-of-phase with T_{CO_2}. The amplitude of the oscillation varied from a minimum of 0.015 cm at 0.25 s after ignition to a maximum of 0.09 cm 1.5 s after ignition.

VII. Discussion

Comparing the results acquired via path-integrated measurements of CO and CO_2 absorbance spectra reveals several interesting observations about the diagnostics presented and the thermochemical structure of HMX flames burning in air. First, the results indicate that the CO-based temperature diagnostic is insensitive to line-of-sight non-uniformities

that are encountered in these flames and is therefore capable of providing accurate measurements of the core flame conditions. This is supported by the fact that T_{CO} was within ≈117 K of the adiabatic flame temperature and agrees well with thermocouple measurements presented in the literature [23], especially given the large uncertainty of thermocouple measurements at the temperatures of interest here. Second, the combination of CO- and CO_2-based results suggest that the gas temperature is hottest in the flame core and cooler (on average) in the surrounding shroud of HMX-air combustion products. This is supported, perhaps most clearly, by the fact that T_{CO_2} is nearly 600 K lower than T_{CO}. This can be explained by recognizing that CO should predominantly exist in the flame core since it will be oxidized to CO_2 in regions where oxygen/air have diffused into the flame and, thus, it should also not exist in large quantities in the cold boundary layer surrounding the flame. In contrast, CO_2 should be biased towards the regions where oxygen/air have diffused into the flame (since HMX is fuel rich) and to the colder boundary layer gas surrounding the flame since it is fully oxidized. This is further supported by several key results. 1) The measured column density of CO_2 is consistent with significant diffusion and entrainment of air into the flame. For example, assuming an absorbing path length of 15 mm (as estimated from Fig. 2), the measured steady-state mole fraction of CO_2 at the measurement location is 0.12 which is significantly larger than that expected from combustion of pure HMX (i.e., 0.05 at equilibrium) [23]. 2) The column density of CO_2 oscillated ≈180 degrees out-of-phase with T_{CO_2}. This is consistent with CO_2 existing at lower temperatures (on average) when CO_2 is produced in the largest quantities (i.e., when diffusion from atmospheric oxygen into the flame is most significant). 3) An oscillation was not observed in the measured T_{CO} which is consistent with measuring the equilibrium flame temperature of pure HMX as it should not be affected by the flame instability. 3) Last, the systematic error between the measured and best-fit absorbance spectra of CO_2 strongly suggests that, at the measurement location, CO_2 existed over a wide range of temperatures along the measurement line-of-sight.

VIII. Conclusions

The development and application of a mid-infrared ultrafast-laser-absorption diagnostic for measurements of temperature, CO, and CO_2 in combustion gases was presented. The first single-shot, single-spectrum (i.e., no spatial averaging), ultrafast measurements of temperature and species were demonstrated, thereby marking an important step towards acquiring 1D thermometry and concentration measurements with sub-picosecond time resolution.

This diagnostic was applied to characterize HMX flames burning in air at 1 atm. The results demonstrate that comparing temperature measurements acquired via the path-integrated absorbance spectra of multiple species can provide improved insight into the flame structure. Combining measurements of temperature and column density from CO and CO_2 spectra provided improved insight into the line-of-sight non-uniformities encountered in HMX flames burning in air. The results suggest that the CO-based temperature measurements are representative of the conditions in the flame core, while CO_2-based temperature measurements are heavily biased towards the outer regions of the flame. The results also suggest that the highest temperatures exist in the core of the HMX flame, with temperatures decreasing (on average) towards the boundary layer between air and HMX combustion products.

Acknowledgments

Funding for this work was provided by AFOSR Grant FA9550-18-1-0210 with Dr. Mitat Birkan as program manager and NSF CBET Grant 1834972. The authors would like to thank Austin McDonald for technical advice regarding the development of the broadband spectral-fitting routine used in this work.

References

[1] Goldenstein, C. S., Spearrin, R. M., Jeffries, J. B., and Hanson, R. K., "Infrared laser-absorption sensing for combustion gases," *Progress in Energy and Combustion Science*, Vol. 60, 2017, pp. 132–176.

[2] Neupane, S., Loparo, Z., Barak, S., Pryor, O., Ninnemann, E., and Vasu, S., "MHz-rate measurements of time-resolved species concentrations in shock heated chemical weapon simulants," *RAPID 2018 - 2018 IEEE Research and Applications of Photonics In Defense Conference*, 2018, pp. 291–294.

[3] Mathews, G. C., and Goldenstein, C. S., "Wavelength-modulation spectroscopy for MHz thermometry and H_2O sensing in combustion gases of energetic materials," *AIAA Scitech 2019 Forum*, 2019, p. 1609.

[4] Sanders, S. T., Wang, J., Jeffries, J. B., and Hanson, R. K., "Diode-laser absorption sensor for line-of-sight gas temperature distributions," *Applied Optics*, Vol. 40, No. 24, 2001, pp. 4404–4415.

[5] Rein, K. D., Roy, S., Sanders, S. T., Caswell, A. W., Schauer, F. R., and Gord, J. R., "Measurements of gas temperatures at 100 kHz within the annulus of a rotating detonation engine," *Applied Physics B: Lasers and Optics*, Vol. 123, No. 3, 2017, p. 88.

[6] Strand, C. L., Ding, Y., Johnson, S. E., and Hanson, R. K., "Measurement of the mid-infrared absorption spectra of ethylene (C_2H_4) and other molecules at high temperatures and pressures," *Journal of Quantitative Spectroscopy and Radiative Transfer*, Vol. 222-223, 2019, pp. 122–129.

[7] Sanders, S. T., "Wavelength-agile fiber laser using group-velocity dispersion of pulsed super-continua and application to broadband absorption spectroscopy," *Applied Physics B: Lasers and Optics*, Vol. 75, No. 6-7, 2002, pp. 799–802.

[8] Göran Blume, N., and Wagner, S., "Broadband supercontinuum laser absorption spectrometer for multiparameter gas phase combustion diagnostics," *Optics Letters*, Vol. 40, No. 13, 2015, p. 3141.

[9] Schroeder, P. J., Wright, R. J., Coburn, S., Sodergren, B., Cossel, K. C., Droste, S., Truong, G. W., Baumann, E., Giorgetta, F. R., Coddington, I., Newbury, N. R., and Rieker, G. B., "Dual frequency comb laser absorption spectroscopy in a 16 MW gas turbine exhaust," *Proceedings of the Combustion Institute*, Vol. 36, No. 3, 2017, pp. 4565–4573.

[10] Draper, A. D., Cole, R. K., Makowiecki, A. S., Zdanawicz, A., Mohr, J., Marchese, A., Hoghoogi, N., and Rieker, G. B., "Progress toward dual frequency comb spectroscopy in a rapid compression machine," *Optics Express*, Vol. 27, No. 8, 2019, pp. 10814–10825.

[11] Stauffer, H. U., Walsh, P. S., Roy, S., and Gord, J. R., "Time-resolved optically gated absorption (TOGA) spectroscopy: A background-free, single-shot broadband absorption method for combusting flows," *AIAA Scitech 2019 Forum*, 2019, p. 1607.

[12] An, X., Caswell, A. W., and Sanders, S. T., "Quantifying the temperature sensitivity of practical spectra using a new spectroscopic quantity: Frequency-dependent lower-state energy," *Journal of Quantitative Spectroscopy and Radiative Transfer*, Vol. 112, No. 5, 2011, pp. 779–785.

[13] Tancin, R. J., Chang, Z., Gu, M., Radhakrishna, V., Lucht, R. P., and Goldenstein, C. S., "Ultrafast-laser-absorption spectroscopy for single-shot, mid-infrared measurements of temperature, CO, and CH_4 in flames," *arXiv preprint*, 2019.

[14] Tancin, R. J., Spearrin, R. M., and Goldenstein, C. S., "2D mid-infrared laser-absorption imaging for tomographic reconstruction of temperature and carbon monoxide in laminar flames," *Optics Express*, Vol. 27, No. 10, 2019, p. 14184.

[15] Wei, C., Pineda, D. I., Goldenstein, C. S., and Spearrin, R. M., "Tomographic laser absorption imaging of combustion species and temperature in the mid-wave infrared," *Optics Express*, Vol. 26, No. 16, 2018, p. 20944.

[16] Girard, J. J., Spearrin, R. M., Goldenstein, C. S., and Hanson, R. K., "Compact optical probe for flame temperature and carbon dioxide using interband cascade laser absorption near 4.2 μm," *Combustion and Flame*, Vol. 178, 2017, pp. 158–167.

[17] Lee, D. D., Bendana, F. A., Schumaker, S. A., and Spearrin, R. M., "Wavelength modulation spectroscopy near 5 μm for carbon monoxide sensing in a high-pressure kerosene-fueled liquid rocket combustor," *Applied Physics B: Lasers and Optics*, Vol. 124, No. 5, 2018, p. 77.

[18] Rothman, L. S., Gordon, I. E., Barber, R. J., Dothe, H., Gamache, R. R., Goldman, A., Perevalov, V. I., Tashkun, S. A., and Tennyson, J., "HITEMP, the high-temperature molecular spectroscopic database," *Journal of Quantitative Spectroscopy and Radiative Transfer*, Vol. 111, No. 15, 2010, pp. 2139–2150.

[19] Hargreaves, R. J., Gordon, I. E., Rothman, L. S., Tashkun, S. A., Perevalov, V. I., Lukashevskaya, A. A., Yurchenko, S. N., Tennyson, J., and Müller, H. S., "Spectroscopic line parameters of NO, NO_2, and N_2O for the HITEMP database," *Journal of Quantitative Spectroscopy and Radiative Transfer*, Vol. 232, No. 2, 2019, pp. 35–53.

[20] Goldenstein, C. S., Schultz, I. A., Jeffries, J. B., and Hanson, R. K., "Two-color absorption spectroscopy strategy for measuring the column density and path average temperature of the absorbing species in nonuniform gases," *Applied Optics*, Vol. 52, No. 33, 2013, pp. 7950–7962.

[21] Finlinson, J. C., Parr, T., and Hanson-Parr, D., "Laser recoil, plume emission, and flame height combustion response of HMX and RDX at atmospheric pressure," *Symposium (International) on Combustion*, Vol. 25, Elsevier, 1994, pp. 1645–1650.

[22] Lee, D. D., Bendana, F. A., Nair, A. p., Spearrin, R. M., Schumaker, S. A., and Danczyk, S. A., "Laser absorption of carbon dioxide at the vibrational bandhead near 4.2 μm in high-pressure rocket combustion environments," *AIAA Scitech 2020 Forum*, 2020, pp. 1–7.

[23] Tang, C.-J., Lee, Y. J., Kudva, G., and Litzinger, T. A., "A study of the gas-phase chemical structure during CO_2 laser assisted combustion of HMX," *Combustion and flame*, Vol. 117, No. 1-2, 1999, pp. 170–188.